Journal of Materials Research and Technology 33 (2024) 8887–8894

Contents lists available at ScienceDirect

Journal of Materials Research and Technology

journal homepage: www.elsevier.com/locate/jmrt

Effects of electrolyte flow direction on height difference in electroplated Cu microstructures for fine-pitch RDL

Sangyeun Park [a,1], Doheon Koo [a,1], Yeongu Choi [a], Junyoung Park [a], Hongyun So [a,b,*]

[a] Department of Mechanical Engineering, Hanyang University, Seoul, 04763, South Korea
[b] Institute of Nano Science and Technology, Hanyang University, Seoul, 04763, South Korea

ARTICLE INFO

Handling editor: Prof. M Meyers

Keywords:
Advanced packaging
Redistribution layer
Electroplating
Fine-pitch patterning
Packaging reliability

ABSTRACT

As demand for high-performance and efficient semiconductor chips surges, advanced packaging technologies, such as heterogeneous integration and vertical stacking, are becoming increasingly significant. Among these, the redistribution layer (RDL), essential for connecting chips or packaging elements, is being designed with finer line/space dimensions to meet the growing requirements for I/O access. However, as the width of copper lines decreases to several microns, various fabrication errors arise. Notably, variation in electroplated copper height becomes a significant issue, impacting the overall process. This study analyzes the height deposition differences in copper electroplating that occur at fine-pitch lines (width: 3–11 μm) and proposes a method to mitigate height deviations by adjusting the flow direction of the electrolyte. The results indicate that the deposition height difference between the 3 μm and 11 μm width patterns was reduced from 40% to less than 10%, demonstrating improved reliability in the RDL process by enhancing the uniformity of plating heights across both wide and narrow patterns.

1. Introduction

As artificial intelligence becomes increasingly important in global industries, advanced semiconductor packaging technology is gaining attention as a key enabler for high-performance computer chips [1]. Consequently, the on-package integration of multiple dies with varying functionalities and performance levels, achieved by partitioning the functions of existing chips, has been widely adopted in commercial products [2]. Heterogeneous integration, a crucial system functional integration technology, significantly influences the performance and reliability of semiconductor packaging through the implementation of various structures that account for thermal, electrical, and mechanical characteristics. Among these structures, vias (interconnections between levels) [3], interposers (e.g., through-silicon vias, through-glass vias) [4], and bumps (e.g., microbumps, C4 bumps) [5,6] are used to efficiently transmit signals and power between chips and substrates in the vertical direction. In particular, redistribution layers (RDLs), which reroute I/O access to different parts of the chip via horizontal connections and enable the attachment of microbumps to the die, are essential for efficiently distributing signals and power among chips [7].

These interconnection structures must provide exceptional mechanical stability, excellent heat dissipation, and maintain high integration density within a small footprint while minimizing signal loss. As I/O density within chips increases, the complexity of RDL wiring for chip-to-chip connections has also escalated, leading to narrower linewidths and making heat and mechanical stress management more challenging. Furthermore, the need for effective defect management during the manufacturing process has become increasingly critical. Specifically, the ability to form high-performance copper (Cu) traces with fine linewidths uniformly and defect-free has emerged as a significant challenge, especially as the substrate used in the process continues to grow in size [8]. Consequently, numerous studies have been conducted to implement fine-pitch RDL to enhance performance. Tran et al. fabricated an RDL with a width of 10 μm and a polyimide encapsulation layer, which withstood a current density of 1×10^6 A/cm^2 [9]. Meanwhile, Tseng et al. reported an RDL with a linewidth of 2 μm fabricated through electroplating, capable of carrying a high current density of 3×10^6 A/cm^2 [10]. However, further research is needed to predict, control, and reduce process defects for these methods to be applicable to large-area substrates in industrial settings.

To implement fine-pitch RDL technology, processes capable of forming micro-sized patterns are required. However, significant

* Corresponding author. Department of Mechanical Engineering, Hanyang University, Seoul 04763, South Korea.
E-mail address: hyso@hanyang.ac.kr (H. So).

[1] These authors contributed equally.

https://doi.org/10.1016/j.jmrt.2024.11.178
Received 25 September 2024; Received in revised form 2 November 2024; Accepted 18 November 2024
Available online 19 November 2024
2238-7854/© 2024 The Authors. Published by Elsevier B.V. This is an open access article under the CC BY-NC-ND license (http://creativecommons.org/licenses/by-nc-nd/4.0/).

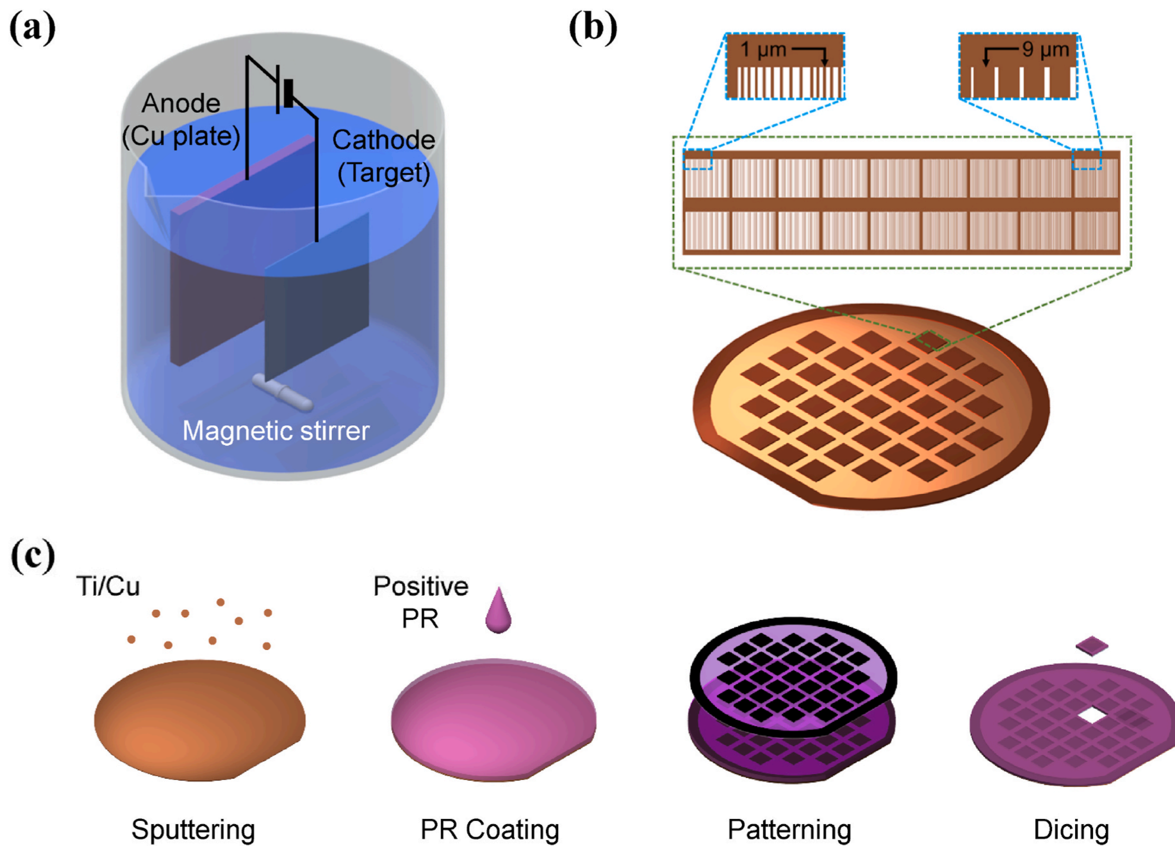

Fig. 1. Pretreatment setup for the electroplating process: (a) electroplating setup, (b) micro-patterns with varying linewidths and spacing, and (c) fabrication process of cathode target.

technical challenges arise in creating fine-pitch patterns during lithography [11–13], etching [14,15], and electroplating [16,17]. Among these processes, Cu electroplating is crucial for constructing electrical circuits in RDL. When electroplated Cu features are formed at micron scales, various fabrication problems, such as delamination [18–20], defects [21–23], and variations in plating height [24–26] occur. Among them, variations in Cu plating height are critical issues that encompass a broader range of challenges faced during the plating process. For instance, when RDLs or other components are stacked with differing plating heights, fabrication reliability diminishes due to flatness issues, necessitating costly chemical mechanical polishing (CMP). Additionally, during the CMP process, the area of Cu in contact with the substrate is reduced, particularly when the width of the electroplated Cu is narrow, resulting in poor adhesion and an increased risk of delamination. Therefore, precise control over plating height during the electroplating process is essential to eliminate the need for CMP and enhance fabrication reliability.

In single-layer RDL, Cu lines of varying widths can be distributed based on circuit design and the pads connected to the bumps. This paper analyzes the deviation in deposition height relative to the width of the Cu lines in the fine-pitch region (3–11 μm). The electroplating method employed is the semi-additive process, which enhances the reliability of fine-pitch RDL. Additionally, ion transport within the pattern is analyzed using computational fluid dynamics (CFD) simulations under various electrolyte flow conditions. Based on the results, a method is proposed to reduce deviation through adjustments in current density and electrolyte flow.

2. Experimental method

2.1. Preparation for electroplating process

The electroplating bath, equipped with a power source and a magnetic stirrer, was prepared as shown in Fig. 1(a). The anode was connected to a bulk Cu plate with an area of 5 cm × 5 cm, while the cathode was connected to the target to be electroplated. A Cu electroplating solution with a concentration of 50 g/L (MICROFAB Cu 520, Electroplating Engineers of Japan Ltd.) was used. The power supply was operated under constant current conditions, and a magnetic stirrer was employed to regulate the flow of the solution. As illustrated in Fig. 1(b), the microstructure patterns were designed as line arrays, with each pattern measuring 0.5 mm in length, widths ranging from 3 to 11 μm, and distances between patterns varying from 1 to 9 μm. Each pattern was arranged sequentially with widths of 3, 4, 5, 6, 7, 8, 9, 10, and 11 μm, maintaining equal spacing between patterns. Fig. 1(c) depicts the overall fabrication process used to prepare the sample for cathode target. First, Cu and titanium (Ti) seed layers, with thicknesses of 200 nm and 50 nm, respectively, were deposited on a silicon substrate through sputtering. Next, positive-type photoresist (PR) was applied to a target thickness of 8.5 μm using a spin coater. A chrome photomask with line patterns of 3–11 μm width was then placed over the sample and exposed to UV light for 15 s. Finally, the areas to be electroplated with Cu were revealed through a development process. The developed sample was rinsed with deionized (DI) water, dried with nitrogen (N_2) gas, and cut into the desired size to complete the preparation for electroplating.

2.2. Measurement

Scanning electron microscopy (SEM; Quattro ESEM, Thermo Fisher Scientific Inc.) was employed to observe the microstructure arrays of

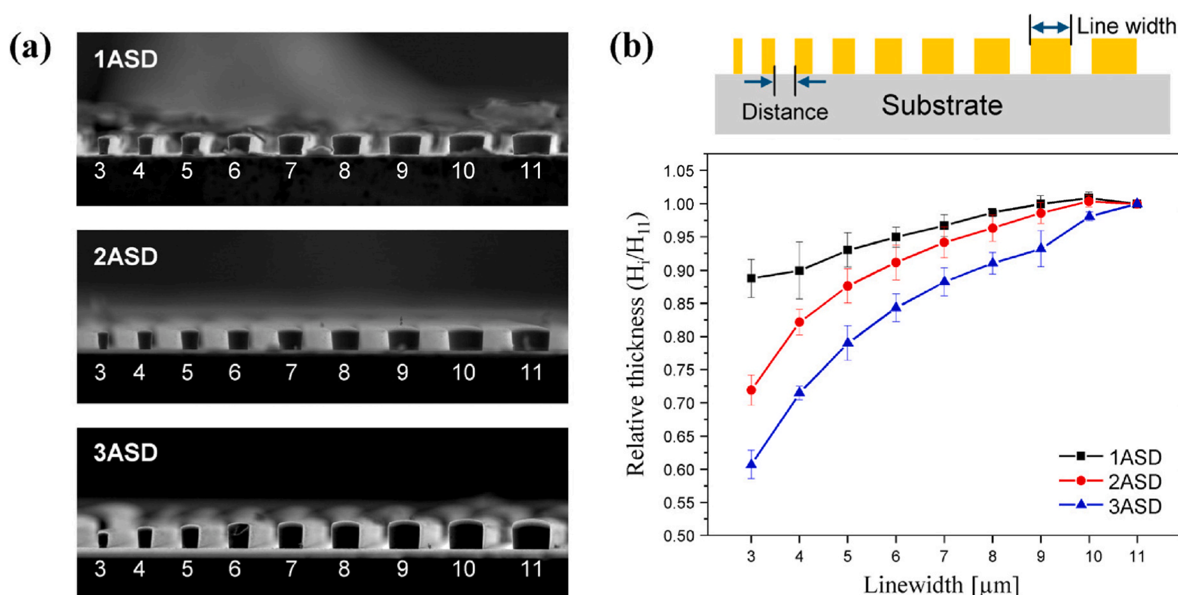

Fig. 2. Morphology analysis of Cu microstructures: (a) SEM images and (b) comparison of relative thicknesses at different current densities.

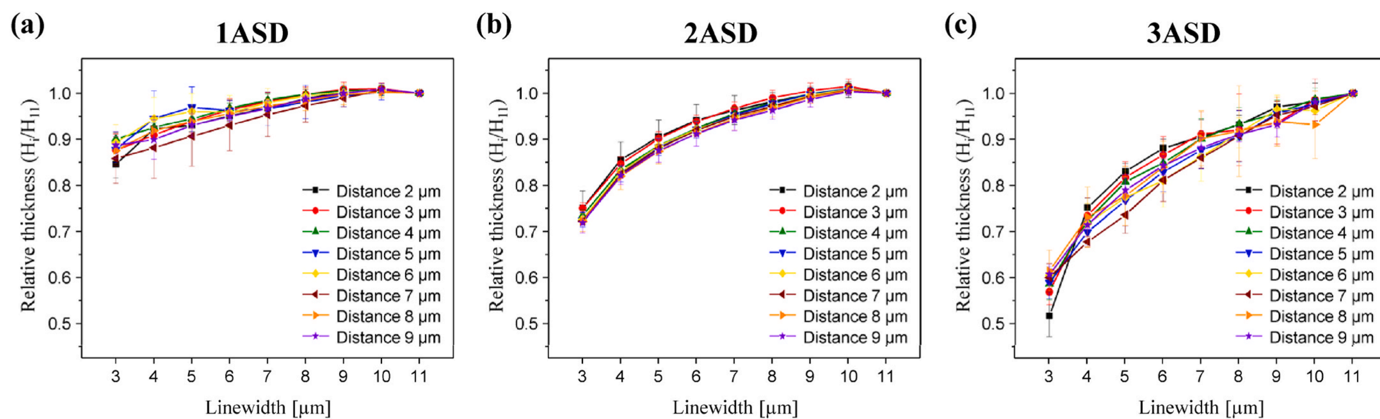

Fig. 3. Deposition relative thickness under process current densities of (a) 1 ASD, (b) 2 ASD, and (c) 3 ASD, with respect to various inter-pattern distances.

plated Cu. The heights and surface topographies of the microstructures were quantitatively measured at a scan speed of 1 mm/min using a surface profilometer (Dektak XT, BRUKER) with a resolution of 1 Å.

3. Results and DISCUSSION

3.1. Experimental results for current density

To analyze the effect of current density on the microstructure morphology resulting from electroplating, the process was first conducted without stirring the solution. The plating process began by wetting the sample with DI water to enhance surface wettability, followed by immersion in the electroplating bath. Electroplating was then carried out at current densities of 1, 2, and 3 A/dm^2 (ASD), with the desired height achieved by adjusting the plating time accordingly. The electroplating process lasted approximately 30 min at 1 ASD, 12 min at 2 ASD, and about 8 min at 3 ASD.

As shown in Fig. 2, the height uniformities of microstructure arrays were analyzed with respect to different electroplating current densities. The experimental results indicated that height uniformity decreased as the current density increased during electroplating (Fig. 2(a)). To quantitatively compare the deposition heights under various process current densities, the relative thickness was defined as follows:

$$Relative\ thickness = \frac{H_i}{H_{11}} \tag{1}$$

where H_{11} represents the height of the deposited Cu microstructure with a width of 11 μm, while H_i represents the height of the Cu microstructure with a width of i μm. When comparing the deposition height in relation to process current density, the minimum relative thickness for the 9 μm-width pattern was 0.89 under the 1 ASD condition, decreasing to 0.61 under the 3 ASD condition, leading to a larger deviation (Fig. 2(b)). Accordingly, as the linewidth narrowed, the relative thickness decreased, further increasing the overall deposition deviation. Furthermore, the experimental results indicated that the height uniformity of Cu microstructures improved as the current density decreased. At higher current densities, local deposition rate of Cu^{2+} ion can be distinct by structure, resulting in a significantly poor uniformity [27].

To analyze the effect of the distance between microstructures, the relative thickness results at distances ranging from 2 μm to 9 μm were compared, as shown in Fig. 3. It was observed that when the current density was set from 1 to 3 ASD, the relative thickness showed a decreasing trend as the pattern width narrowed across the entire range of inter-pattern distances. Especially, under the 2 ASD condition shown in Fig. 3(b), the difference in relative thickness increased as the distance between patterns expanded. However, the effect of inter-pattern

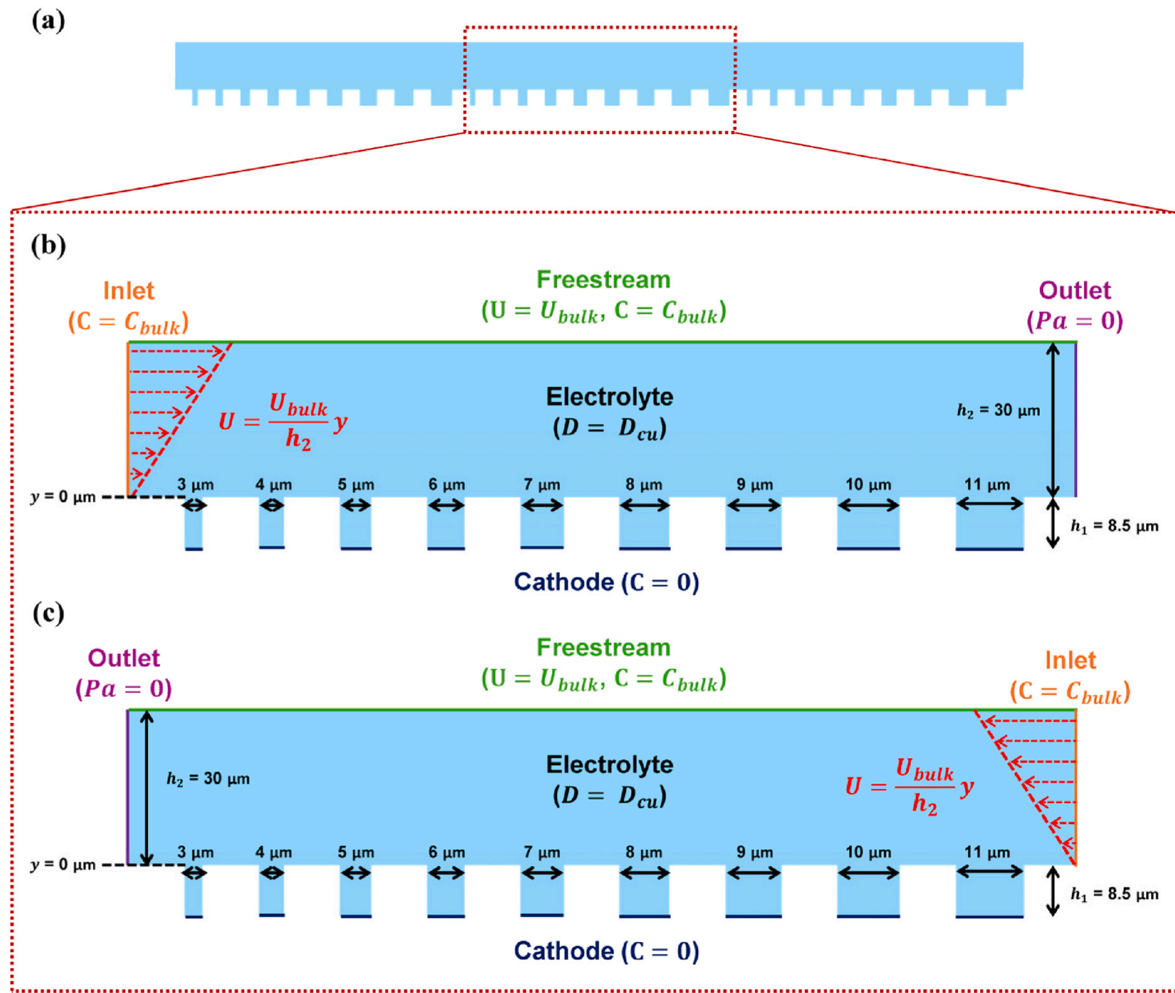

Fig. 4. Schematic of the simulation domain for ion transport in micro-patterns: (a) total domain, (b) direction I, and (c) direction II.

distance on deposition height was insignificant compared to current density. Consequently, experimental analysis of Cu electroplating under various deposition conditions revealed that height uniformity deteriorates with increasing current density. This poses a significant challenge in reducing process time by increasing the process current density.

3.2. Simulation of concentration distribution in pattern with electrolyte flow

To address the deposition thickness difference between narrow and wide patterns, a compensation method is necessary to increase the deposition rate at the bottom of the narrow pattern while maintaining that of the wide pattern. The deposition thickness of electroplated Cu can be expressed as follows based on Faraday's law of electrolysis [28]:

$$h_{dep} = \frac{|i_{loc}| t M_{cu}}{z F \rho_{cu}} \quad (2)$$

where h_{dep} is deposition thickness, i_{loc} is local current density on electrode surface, t is electroplating time, M_{cu} is molar mass of Cu, z is number of electrons, F is Faraday constant, and ρ_{cu} is density of Cu. Based on the above expression, the deposition rate increases in proportion to the local current density on the electrode surface, which can be expressed by the Nernst–Planck equation [29–31]:

$$i_{loc} = -zFD_{cu}\nabla C|_{on\ electrode} - zFUC - F^2 z^2 u_m C \nabla \phi|_{on\ electrode} \quad (3)$$

where D_{cu} is diffusion coefficient of Cu ions, U is velocity of electrolyte, u_m is mobility of the Cu ions, and ϕ is electric potential. Assuming that the electric potential gradient near the narrow and wide pattern electrodes is identical by supporting electrolyte [29], this expression highlights two key points: first, that the current density varies based on the concentration distribution within the pattern; and second, that enhancing ion transport in the narrow pattern reduces the thickness difference, as the current density increases with the concentration and its gradient near the electrode. Therefore, analyzing the concentration distribution within the pattern is essential for achieving height uniformity in deposition thickness for both narrow and wide patterns.

To simulate ion transport in an electrolyte domain with various widths of patterns, a multi-physics CFD simulation was conducted by coupling the laminar flow module for the velocity field with the transport of diluted species module for the concentration field. In this simulation, ion transport by electro-migration was excluded, as the current density difference was negligible when the same voltage was applied to both the narrow and wide patterns. The laminar flow module utilized the steady-state Navier-Stokes equation under the assumption of incompressible flow [32].

$$\rho(\mathbf{U} \bullet \nabla)\mathbf{U} = \nabla \bullet \left[-\mathrm{p}\mathbf{I} + \mu\left(\nabla \mathbf{u} + (\nabla \mathbf{u})^T\right) \right] \quad (4)$$

where ρ is density of electrolyte, **U** is velocity vector, p is pressure, and μ is dynamic viscosity of electrolyte. For the transport of the diluted species module, the advection-diffusion equation assuming a steady and incompressible flow was used [33].

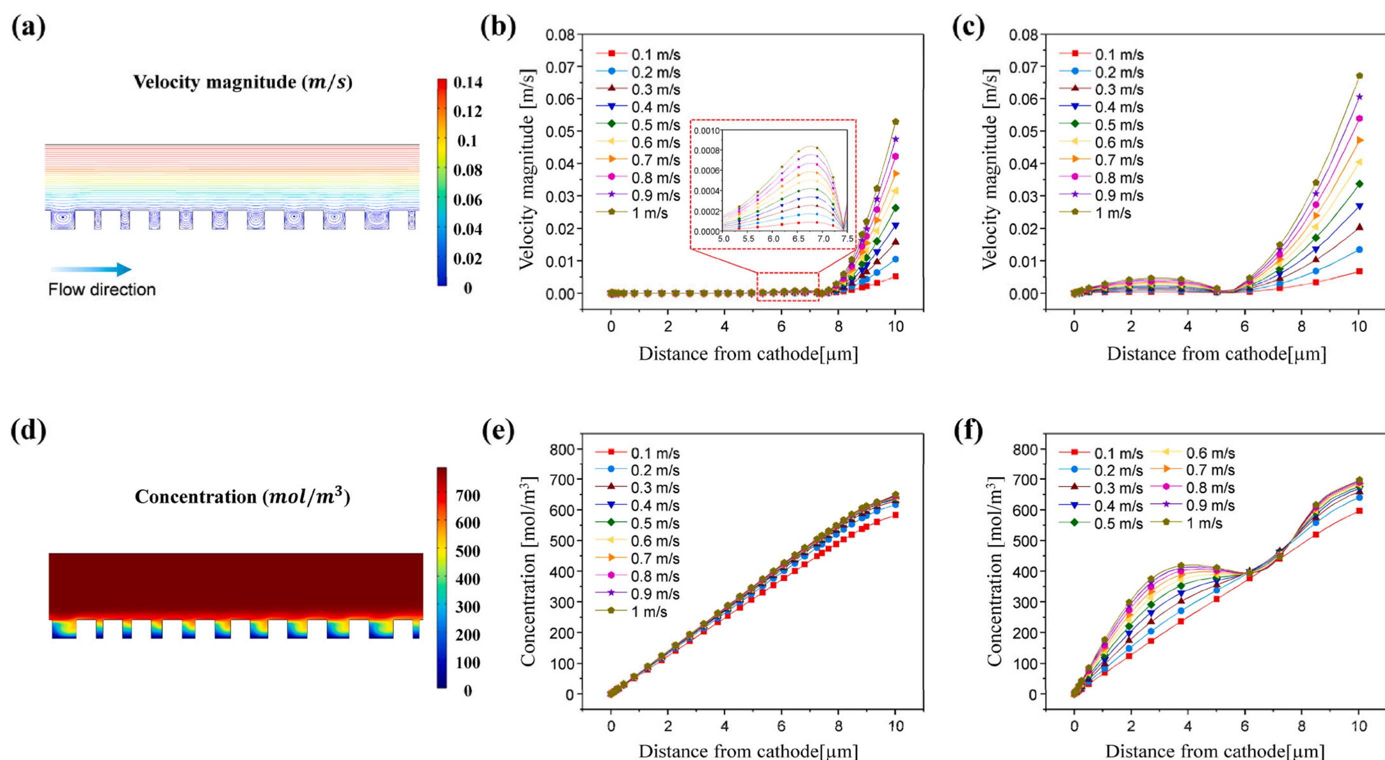

Fig. 5. Simulation results in the direction I: (a) electrolyte flow streamlines, (b) velocity profile in the narrow pattern, (c) velocity profile in the wide pattern, (d) concentration distribution contour, (e) concentration distribution in the narrow pattern, and (f) concentration distribution in the wide pattern.

$$\nabla \bullet (- D_{cu} \nabla C) + \mathbf{U} \bullet \nabla C = 0 \tag{5}$$

To replicate real substrate and electrolyte conditions, the simulation domain consisted of three sets of areas with pattern widths varying from 3 to 11 μm, spaced at a constant interval of 9 μm, as shown in Fig. 4(a). The flow of electrolyte above the patterns was simplified to a linear profile due to the no-slip boundary conditions and the bulk freestream velocity (U_{bulk}). Additionally, to examine the differences in ion transport

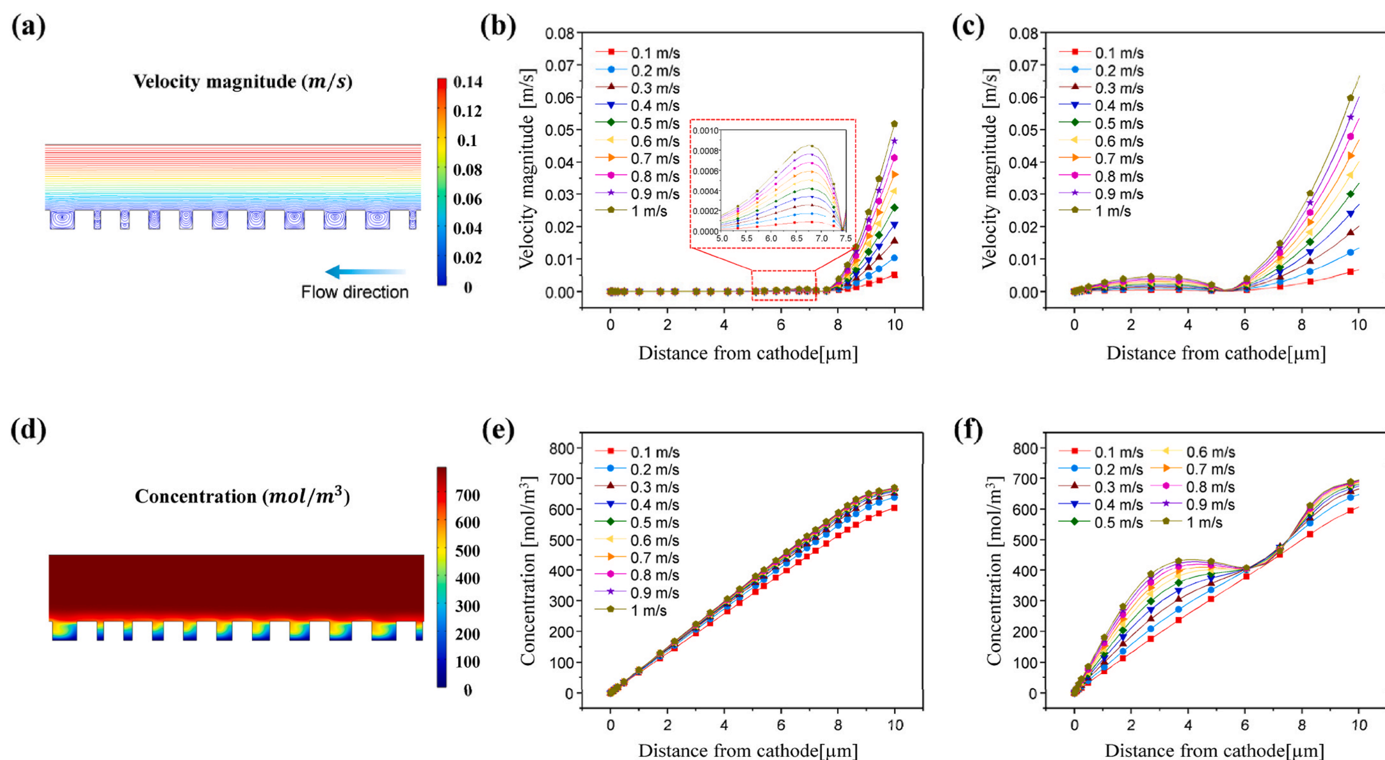

Fig. 6. Simulation results in the direction II: (a) electrolyte flow streamlines, (b) velocity profile in the narrow pattern, (c) velocity profile in the wide pattern, (d) concentration distribution contour, (e) concentration distribution in the narrow pattern, and (f) concentration distribution in the wide pattern.

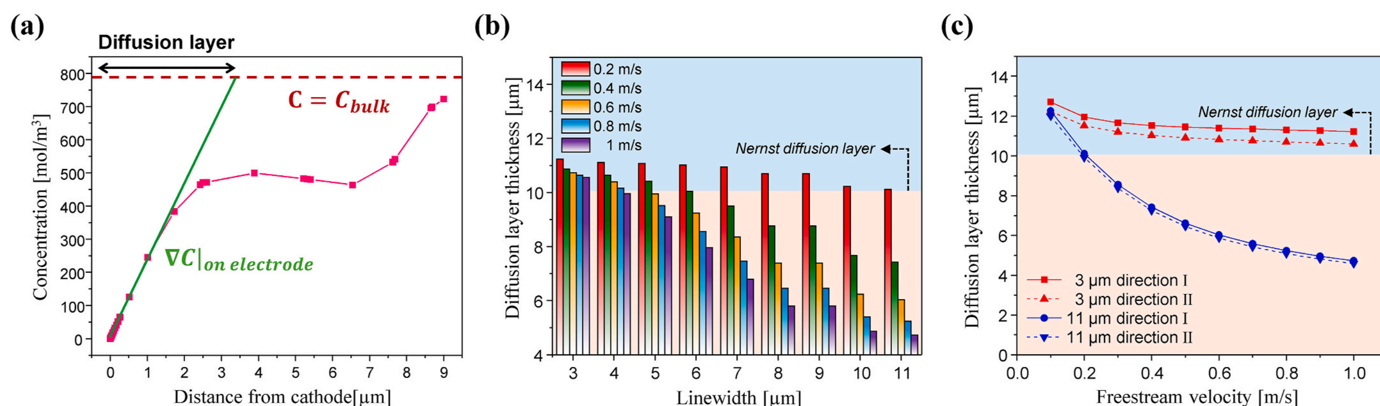

Fig. 7. (a) Definition of diffusion layer, (b) diffusion layer thickness according to linewidth for direction I, and (c) comparison of direction I and direction II.

between wide and narrow patterns, simulations were conducted in two flow directions: flow from the narrow pattern side was considered the direction I (Fig. 4(b)), while flow from the wide pattern side was regarded as the direction II (Fig. 4(c)). Finally, the bulk concentration (C_{bulk}) was fixed at 787 mol/m^3 and the diffusion coefficient of Cu ions was calculated using the Stokes-Einstein relation as follows [34]:

$$D_{cu} = \frac{\kappa_B T}{6\pi\mu r} \tag{6}$$

where κ_B is Boltzmann's constant, T is the absolute temperature, and r is the radius of the Cu ion.

Fig. 5 presents the simulation results for the direction I. First, the results for the velocity field (Fig. 5(a)) indicate different flow behaviors within the wide and narrow patterns. In the narrow pattern, the flow passed without penetrating the pattern, whereas a large vortex was formed within the pattern, enabling the flow to approach the bottom in the wide pattern. When quantitatively comparing the velocity magnitude profile at the center of the patterns, a weak vortex was visible at the top of the 3 μm width pattern (approximately 7 μm from the bottom) (inset graph in Fig. 5(b)), while the velocity magnitude was distributed throughout the entire 11 μm width pattern (Fig. 5(c)). The strength of the vortex inside the pattern tended to increase as the external free velocity rose, but the ratio of the velocity within the pattern to the bulk velocity remained invariant regardless of the freestream velocity magnitude (0.084% for the 3 μm pattern and 0.47% for the 11 μm pattern). Additionally, the velocity magnitude above the 11 μm pattern was observed to be more than the narrow side of the pattern due to flow resistance caused by the microstructure of the narrow pattern. These results confirm that transporting ions into the narrow pattern via convection is more challenging when electrolyte flow is present. This trend is clearly illustrated by the concentration distribution of Cu ions within the pattern (Fig. 5(d)). In the narrow pattern (Fig. 5(e)), the concentration gradient appeared linear, as indicated by the rightmost term on the right side of Eq. (3), since ion transport by diffusion was more dominant than that by convection. Furthermore, the concentration gradient remained relatively unchanged even as the strength of the freestream velocity increased. In contrast, within the wide pattern, the concentration increased linearly at low freestream velocities (at 0.1 m/s), but the distribution was changed at high velocities (Fig. 5(f)). At high freestream velocity, concentration rose rapidly at the bottom of the pattern ($y < -6$ μm) and stabilized in the middle region (-6 μm $< y < -1.5$ μm) due to the internal vortex. This concentration distribution exhibited a steep gradient at the bottom and a high concentration within the pattern, enhancing the Cu deposition rate in the wide pattern according to Eqs. (2) and (3).

The simulation results for electrolyte flow in the direction II are shown in Fig. 6. The velocity field results for both the narrow and wide patterns were similar to those observed in the direction I, indicating that flow direction did not affect the velocity profile (Fig. 6(a)–(c)). However, the concentration distribution differed from that in the direction I (Fig. 6(d)). In the narrow pattern (Fig. 6(e)), the concentration was generally higher (670 mol/m^3 at 10 μm from cathode and 1 m/s of velocity) than in the direction I (649 mol/m^3 at same condition of direction II). Additionally, in the wide pattern (Fig. 6(f)), the concentration gradient at the bottom ($y < -6$ μm) and the concentration in the middle region (-6 μm $< y < -1.5$ μm) was also higher (435 mol/m^3 at 10 μm from cathode and 1 m/s of velocity) than in the direction I (420 mol/m^3 at same condition of direction II). This phenomenon occurred because the concentration decreased as Cu ions were transported within the pattern while ions moved from the wider pattern to the next. These results suggest that the difference in ion concentration between the narrow and wide patterns can be compensated depending on the direction of electrolyte flow.

The difference in deposition rate due to concentration distribution within the pattern under various flow conditions can be predicted using Eq. (3). The current density at the electrode is primarily influenced by the diffusion term, which is the first term on the right side of Eq. (3), as electrolyte flow does not reach the area near the cathode. In other words, the current density near the cathode is directly affected by the concentration gradient in that region. The property that quantifies the concentration gradient near the cathode is the diffusion layer, defined as the distance required to reach bulk concentration when the concentration is distributed in proportion to the gradient at the bottom (Fig. 7(a)) [35]. Accordingly, the deposition rate by diffusion can be compared to be almost the same when the thickness of the diffusion layer is similar. However, there are limitations to assessing the deposition rate based on the diffusion layer thickness only. In actual electrochemical deposition, the deposition rate does not increase infinitely as the diffusion layer thickness decreases because there is a limit to the reaction rate [36,37]. Therefore, the concentration gradient that affects the deposition rate converges by process parameters such as current density, bulk ion concentration, and other electrochemical properties. This convergence state can be estimated by calculating Nernst diffusion layer thickness. The Nernst diffusion layer can be mathematically calculated using Fick's law as follows [36,37]:

$$\delta = -\frac{zFDC}{i_{applied}} \tag{7}$$

Where δ is the diffusion layer thickness and $i_{applied}$ is applied current density. When the diffusion layer was formed below the Nernst diffusion layer thickness, the deposition rate no longer increases and converges at constant value by the applied current density. Under 3 ASD conditions, the Nernst diffusion layer thickness for this process was approximately 10.12 μm. In contrast, when the diffusion layer thickness exceeds this threshold, a smaller diffusion layer thickness induces an increased deposition rate.

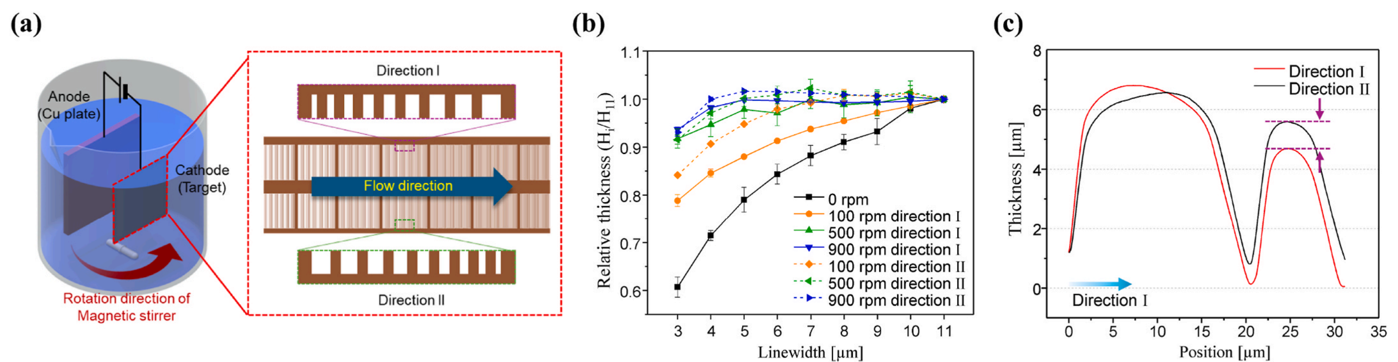

Fig. 8. (a) Definition of flow direction by the rotation of the magnetic stirrer, (b) Deposition trends for various linewidth patterns under different electrolyte flow conditions and (c) surface topography analysis results.

The diffusion layer thickness within the narrow and wide patterns is shown in Fig. 7 for electrolyte flow in the direction I (Fig. 7(b)) and the difference in diffusion layer thickness depending on flow direction (Fig. 7(c)). As the flow velocity increased, the diffusion layer thickness decreased, with increasing pattern width, as shown in Fig. 7(b). It is noteworthy that even within the same pattern width, the diffusion layer thickness can fall below the Nernst diffusion layer thickness as the flow rate increases. In the narrow pattern (3 μm), the diffusion layer thickness was shorter when the flow was in the direction II, as the concentration at the top of the pattern was higher than that in the direction I (Fig. 7(c)). Additionally, in this case, the diffusion layer thicknesses in all conditions were greater than Nernst diffusion layer thickness; thus, the deposition rate increased when the flow was in the direction II. Similarly, in the wide pattern (11 μm), the diffusion layer also became shorter in the direction II. However, when the electrolyte velocity exceeded 0.2 m/s, the diffusion layer thickness became below the Nernst diffusion layer thickness, so the deposition rate no longer increased regardless of the flow direction and velocity. As a result, difference in deposition height between the narrow and wide patterns varied depending on the deposition rate in narrow pattern, confirming that the difference in deposition height can be reduced by plating under flow of direction II.

3.3. Experimental results with electrolyte flow

To verify and apply the CFD results, additional experimental studies were conducted using flow-assisted electroplating. With electrolyte flow by the magnetic stirrer, the electrolyte in the beaker generated a tangential flow around the rotation axis [38], and this tangential flow can correspond to the flow in the simulation model from the perspective of the cathode. The flow direction was defined by fixing tangential flow direction and altering the arrangement of the cathode pattern. Under conditions identical to the simulation, flow from the narrow pattern side was considered the direction I and flow from the wide pattern side was considered the direction II, as shown in Fig. 8(a). Fig. 8(b) shows the comparison of relative thicknesses of electroplated Cu microstructure arrays under different flow conditions. When there was no flow, the relative thickness significantly decreased as the line width narrowed. However, when flow was applied, the deviation decreased. This reduction was attributed to the diffusion layer thickness becoming shorter in narrow pattern by flow. Furthermore, the relative thickness deviation was smaller under direction II than under direction I. Comparing this with the diffusion layer of the simulation results, it can be observed that the plating height remains constant when the flow velocity and linewidth was sufficient to reduce the diffusion layer thickness below the Nernst diffusion layer thickness. However, if the flow velocity was slower or the width is narrow, the plating height formed lower. Additionally, the topography of the deposited copper traces (Fig. 8(c)) confirmed that the deposition height increases more significantly in the narrow pattern than in the wide pattern according to flow direction, agreeing with the simulation analysis results which suggested that variations in deposition rate within the narrow pattern can reduce height differences between narrow and wide pattern.

4. Conclusions

In the copper electroplating process for implementing fine-pitch RDL, the impact of substrate pattern width on deposition rates was analyzed. In the absence of electrolyte flow, the deposition rate was varied with pattern width, with narrower patterns (3–6 μm) resulting in lower deposition heights compared to wider patterns (7–11 μm). Furthermore, this deviation in plating height between narrow and wide patterns became more pronounced as the applied current density increases. To address these fabrication errors, CFD simulations were conducted with varying flow directions of the electrolyte over the patterns. The results confirmed that while the velocity profile remained unaffected by the flow direction, the concentration distribution within the pattern varied depending on the flow condition, as the amount of ions penetrating the pattern was influenced by its width. Based on these findings, the difference in deposition height between the narrow and wide pattern can be alleviated by direction of electrolyte flow, improving uniformity. Consequently, in RDL designs with varying pattern widths, fabrication errors related to height deviation can be minimized by optimizing current density and electrolyte flow direction. This optimization is expected to enhance reliability by eliminating the CMP process and reducing fabrication errors in multi-layer RDL processes and packaging integration.

Declaration of competing interest

The authors declare that they have no known competing financial interests or personal relationships that could have appeared to influence the work reported in this paper.

Acknowledgments

This work was supported by the Korea Evaluation Institute of Industrial Technology (KEIT), funded by the Ministry of Trade, Industry, and Energy (MOTIE) of the Republic of Korea (RS-2024-00418263).

References

[1] Smallwood DC, McCloskey P, O'Mathuna C, Casey DP, Rohan JF. Methods for latent image simulations in photolithography with a polychromatic light attenuation equation for fabricating VIAs in 2.5D and 3D advanced packaging architectures. Microsystems Nanoeng 2021;7:39.

[2] Das Sharma D, Pasdast G, Tiagaraj S, Aygün K. High-performance, power-efficient three-dimensional system-in-package designs with universal chiplet interconnect express. Nat. Electron. 2024;7:244–54.

[3] Hong TY, Kim SE, Park JK, Hong SK. Guidelines for area ratio between metal lines and vias to improve the reliability of interconnect systems in high-density electronic devices. Electronics 2023;12:4403.
[4] Salah K. TGV versus TSV: a comparative analysis. In: 2016 3rd int. Conf. Adv. Comput. Tools eng. Appl. IEEE; 2016. p. 49–53.
[5] Cho Y, Hahn M, Jeong H, Jang G. Shear test evaluation of the mechanical reliability of micro bumps in semiconductors, Microsyst. Technol 2022;28:2173–80.
[6] Rahimipour S, Zhang R, Wang K, Skadron K, Rokhani FZB, Stan MR. MTTF enhancement power-C4 bump placement optimization, IEEE trans. Very large scale integr. Off Syst 2019;27:1633–9.
[7] Chen C, Cherng S-J, He C, Chung C-C, Wang S, Huang Y-T, Feng SP. Nanotwinning-assisted structurally stable copper for fine-pitch redistribution layer in 2.5D/3D IC packaging. J Mater Res Technol 2023;27:4883–90.
[8] Wu X, Wang Z, Ma S, Chu X, Li C, Wang W, Jin Y, Wu D. An RDL modeling and thermo-mechanical simulation method of 2.5d/3D advanced package considering the layout impact based on machine learning. Micromachines 2023;14:1531.
[9] Tran D-P, Li H-H, Tseng I-H, Chen C. Enhancement of electromigration lifetime of copper lines by eliminating nanoscale grains in highly <111>-oriented nanotwinned structures. J Mater Res Technol 2021;15:6690–9.
[10] Tseng I-H, Shie K, Tzu-Hung Lin B, Chang C-C, Chen C. Electromigration in 2 μm redistribution lines and Cu-Cu bonds with highly <111>- oriented nanotwinned Cu. In: 2020 IEEE 70th electron. Components technol. Conf. IEEE; 2020. p. 479–84.
[11] Yukimori D, Kunito M, Ishikawa N, Sekiguchi A, Ogata T. Study of i-line photosensitive materials with a wide depth of focus for fine pitch redistribution layers. In: 2021 IEEE 71st electron. Components Technol. Conf. IEEE; 2021. p. 1963–70.
[12] Liu F, Nimbalkar P, Aslani-Amoli N, Kathaperumal M, Tummala R, Swaminathan M. A critical review of lithography methodologies and impacts of topography on 2.5-D/3-D interposers. IEEE Trans. Components, Packag. Manuf. Technol. 2023;13:291–9.
[13] Sato T. Talbot effect immersion lithography by self-imaging of very fine grating patterns. J. Vac. Sci. Technol. B, Nanotechnol. Microelectron. Mater. Process. Meas. Phenom. 2012;30.
[14] Kim SH, Lim ET, Park SY, Chung CW. Two-step cyclic etching of copper thin films using acetylacetone/O_2 gases. ECS J. Solid State Sci. Technol. 2023;12:074010.
[15] Marton M, Ritomsky M, Rehacek V, Michniak P, Behul M, Novak P, Vanco L, Vojs M. Comparison of Al and Cu masks used for patterning boron-doped diamonds in oxygen plasma. J. Micromechanics Microengineering. 2019;29:124004.
[16] Luo V, Xue X-T, Yu K-C, Meng J, Lu H-L, Zhang DW. Method to improve the process efficiency for copper pillar electroplating. J Electrochem Soc 2016;163:E39–42.
[17] Dixit P, Miao J. Aspect-ratio-dependent copper electrodeposition technique for very high aspect-ratio through-hole plating. J Electrochem Soc 2006;153:G552.
[18] Wakeel S, Haseeb ASMA, Hoon KL, Amalina MA. Effects of commercial No-clean flux on reliability of fine pitch flip-chip package with solder bumps and copper pillars. IEEE Trans. Components, Packag. Manuf. Technol. 2022;12:1386–94.
[19] Lee H, Park SK, Jeong K, Jung J, Choi J, Kang U-B, Kim K. Development of fine pitch backside redistribution layer (BRDL) process in fan out panel level packaging (FOPLP). In: 2023 IEEE 73rd electron. Components technol. Conf. IEEE; 2023. p. 515–9.
[20] Seah C, Mridha S, Chan L. Adhesive strength of electroplated copper films. J Mater Process Technol 2001;114:252–6.
[21] Wang F, Zhao Z, Nie N, Wang F, Zhu W. Dynamic through-silicon-via filling process using copper electrochemical deposition at different current densities. Sci Rep 2017;7:46639.
[22] Malta D, Gregory C, Temple D, Knutson T, Wang C, Richardson T, Zhang Y, Rhoades R. Integrated process for defect-free copper plating and chemical-mechanical polishing of through-silicon vias for 3D interconnects. In: 2010 proc. 60th electron. Components Technol. IEEE: Conf.; 2010. p. 1769–75.
[23] Zhu QS, Zhang X, Liu CZ, Liu HY. Effect of reverse pulse on additives adsorption and copper filling for through silicon via. J Electrochem Soc 2019;166:D3006–12.
[24] Ruan W, Chen L, Li Z, Ye T, Ma T, Wang Q. Effects of pattern characteristics on the copper electroplating process. J. Semicond. 2011;32:055010.
[25] Luo C, Lin C, Ye J, Zeng H, Zhou X, Wu C, Zhang Y, Sun J, Guo T, Yan Q. Electroplating of Cu/Sn bumps with ultrafine pitch and high uniformity for micro-LED interconnection. J Mater Sci Mater Electron 2024;35:878.
[26] Zhang H, Zhang N, Fang F. Study of ion transportation and electrodeposition under hybrid agitation for electroforming of variable aspect ratios micro structures. Precis Eng 2021;72:122–43.
[27] Tian W, Li Z, Wang Y, Zhang G. Height uniformity simulation and experimental study of electroplating gold bump for 2.5d/3D integrated packaging. Micromachines 2022;13:1537.
[28] Bard AJ, Faulkner LR. Electrochemical methods: Fundamentals and Applications. New York: John Wiley & Sons; 1980.
[29] Braun TM, John J, Jayaraju N, Josell D, Moffat TP. Simulating the influence of supporting electrolyte concentration on copper electrodeposition in microvias. J Electrochem Soc 2022;169:012502.
[30] Zahraei M, Saidi MS, Sani M. Numerical simulation of electro-deposition process influenced by force convection and migration of ions. J Electroanal Chem 2016; 782:117–24.
[31] Ribeiro MC, Rego LGC, D'Ajello PCT. Diffusion, reaction and forced convection in electrochemical cells. J Electroanal Chem 2009;628:21–6.
[32] Hirsch C. Numerical computation of internal and external flows. Elsevier; 2007.
[33] Stocker T. Introduction to Climate Modelling. Berlin, Heidelberg: Springer Berlin Heidelberg; 2011.
[34] Einstein A. Über die von der molekularkinetischen Theorie der Wärme geforderte Bewegung von in ruhenden Flüssigkeiten suspendierten Teilchen. 1905.
[35] Natarajan D, Van Nguyen T. A two-dimensional, two-Phase, Multicomponent, transient model for the cathode of a proton exchange membrane fuel cell using conventional gas distributors. J Electrochem Soc 2001;148:A1324.
[36] Mehdizadeh S, Dukovic J, Andricacos PC, Romankiw LT, Cheh HY. The influence of lithographic patterning on current distribution in electrodeposition: experimental study and mass-transfer effects. J Electrochem Soc 1993;140:3497–505.
[37] Walker R, Holt NS. Determination of the nernst diffusion layer thickness in the hydroson agitation tank. Surf Technol 1984;22:165–74.
[38] Halász G, Gyüre B, Jánosi IM, Szabó KG, Tél T. Vortex flow generated by a magnetic stirrer. Am J Phys 2007;75:1092–8.